

Computer assisted radiographic characterization of alloimplant materials used as bone substitutes in dentistry

Naglaa Abdel-Wahed^a, Abdel-Wahab S. Ahmed^a, Adel Zein Elabedeen^a,
Shabaan M. Gadallah^b, Nahed H. Solouma^c, and Yasser M. Kadah^{d 1}

^aOral Radiology Dept., Faculty of Oral & Dental Medicine, Cairo University, Egypt

^bFaculty of Veterinary Medicine, Cairo University, Egypt

^cLaser Research Institute, Cairo University, Egypt

^dEmory University/Georgia Tech Biomedical Engineering Dept., Atlanta GA 30322

ABSTRACT

We develop a computerized system for evaluation of alloimplant procedures in dentistry from x-ray images. The goal of this system is to help clinicians make more accurate evaluation of their surgical procedures as well as to guide them in selecting the most appropriate alloimplant material in an objective manner. A study was conducted whereby three types of alloimplant materials were inserted in surgical defects in the tibia of dogs. Each animal had four such defects for the three different materials in addition to a control defect that was intentionally left empty. The defect locations were imaged using x-rays at periodic intervals starting immediately after the operation. The animals were sacrificed at different times after the surgical operation. The acquired images were paired with their correct diagnosis and split into two sets representing the learning and testing data for our computerized system. The plain x-ray films were scanned using a standard film digitizer and standardized in size and intensity using a step wedge that was imaged beside the region of interest. A set of first and second order textural and radiometric parameters were extracted from each alloimplant location outlined by the radiographer to describe its clinical status in a quantitative manner.

Keywords: digital radiology, computer-assisted radiology, alloimplants, subtraction radiography

1. INTRODUCTION

Many disease conditions can affect the bone, to which it acts in a limited manner. Bone tissue can resorb, die, or new bone may be laid down. Small bone defects heal in an uncomplicated manner, which is not the case when the defect is large. In such conditions, restoring normal size, shape and function of the affected bone may need grafting. Grafting procedures imply that various types of graft materials are put into the osseous defect. Bone grafts could be autografts (from the same individual), allografts (from human cadavers and bone banks) such as demineralized freeze-dried bone allograft (DFDBA) and freeze-dried bone allograft (FDBA) and xenograft (bone from a different species) such as deproteinated bovine-derived hydroxylapatite. Synthetic grafts or alloplasts are inert (inactive) materials, which are biologically accepted by the host. Examples include porous hydroxyapatite, polymethylmethacrylate, polyhydroxyethylmethacrylate and bioactive glass (Peterson *et al.*, 1998)¹.

Radiology is essential to the clinician for qualitative evaluation of bone structure. It may provide the only means to assess the success of the grafting procedure. However, only limited information about mineral content and type of tissue formed can be obtained from the subjective examination of radiographs. Limitations of conventional radiography in detecting small bone lesions can be inferred to the presence of structured noise (van der Stelt, 1979)². Such noise consists of all anatomic features other than those of diagnostic interest. It has been shown that its presence greatly limits the visual detectability of structures of diagnostic significance (Revesz, Kundel, and Graber, 1974, Kundel, and Revesz, 1976)^{3,4}.

¹ E-mail: ymk@ieee.org

Digital subtraction radiography is the method by which structured noise is reduced in order to increase the detectability of changes in the radiographic pattern occurring over a period of time (Ziedses des Plantes, 1961, Chow, Hilal, and Niebuhr, 1973, Hardstedt and Welander, 1975, Kundel, and Revesz, 1976, and, Hardstedt, Rundelius, and Welander, 1976)^{4,5,6,7,8}. Problems may arise if images differ in contrast and/or projection, regardless of whether the comparison is done by experts or with automatic computer algorithms (Lehmann et al., 1997)⁹. In 1998, Lehman *et al.* concluded that perspective projection is a reliable model for sequentially acquired radiographs¹⁰. The coordinates of anatomical landmarks are useful for determining the parameters of perspective projection. Local correlation and leaving one out techniques improve the geometrical adjustment as well as observer independence. Registration is nearly independent of the actual position of the landmarks and hence independent of the observer. Hence, the development of a reliable subtraction technique can provide the clinician with accurate information regarding the success of the grafting procedure.

One of the most important tasks in oral radiology is the evaluation and follow up of implant procedures. The radiographers use visual criteria related to radiometric parameters of the alloimplant as well as its radiological opacity to reach a diagnosis from dental x-ray images. Unfortunately, several factors make this diagnostic procedure difficult. For example, the different alloimplant materials have different radiological characteristics, which makes the comparison between different materials impractical. Also, it is not easy to compare radiometric parameters between different images of the same alloimplant material in the follow-up stage. Therefore, a systematic way of evaluating such images to assess the progress in its healing is in demand to solve these problems.

In this work, we develop a computerized system for evaluation of alloimplant procedures in dentistry from x-ray images. The goal of this system is to help clinicians make more accurate evaluation of their surgical procedures as well as to guide them in selecting the most appropriate alloimplant material in an objective manner. A study was conducted whereby three types of alloimplant materials were inserted in surgical defects in the tibia of dogs. Each animal had four such defects for the three different materials in addition to a control defect that was intentionally left empty. The defect locations were imaged using x-rays at periodic intervals starting immediately after the operation. The animals were sacrificed at different times after the surgical operation. The acquired images were paired with their correct diagnosis and split into two sets representing the learning and testing data for our computerized system. The plain x-ray films were scanned using a standard film digitizer and standardized in size and intensity using a step wedge that was imaged beside the region of interest. A set of first and second order textural and radiometric parameters were extracted from each alloimplant location outlined by the radiographer to describe its clinical status in a quantitative manner. The objective of this work is to develop a reliable subtraction technique that can provide the clinician with accurate information regarding the success of the grafting procedure. We describe in detail the implementation steps of this system as well as sample results obtained for different alloimplant materials at various stages of follow-up and demonstrate the potential of such system as an assisting tool to dental radiologists and surgeons.

2. MATERIALS AND METHODS

Selected adult, apparently healthy, male mongrel dogs (weight 15 to 20 kg) were used as recipients for alloimplants. The dogs were randomly allocated into four groups (see Table 1) whereby animals were sacrificed at one week, one month, three months and six months post-surgery and designated as groups I, II, III and IV respectively. For each animal three types of alloimplant materials were used; namely, Bony-Glass® (BECO company, Giza, Egypt) (RBG), Bioactive glass ceramic (BGC), and Allogenic cortical bone graft (CBA). There was also a site where no material was used to act as a control site for this experiment.

Group No.	Duration	Number of dogs
Group I	1 week	4
Group II	1 month	8
Group III	3 months	9
Group IV	6 months	9
TOTAL		30

Table 1. Distribution of dogs according to the duration of the experiment.

2.1. Materials preparation

- RBG is 45S5 resorbable bioactive glass, which particles were composed of 45% SiO₂, 24.5% CaO, 24.5% Na₂O and 6% P₂O₅ by weight percentages and had a size range of 90-600µm (Schepers et al.,1991).
- BGC is crystallized form of BGR and was prepared by heating BGR at 1000°C for 4 hours.
- CBA is cortical bone harvested from the tibiae of donor animals.

The materials were individually packed in double wrapped plastic rolls and sterilized prior to use with 84% ethylene oxide gas for 12 hours at atmospheric pressure and room temperature, then left for another 24 hours in an aeration chamber. At the beginning of surgery the allogenic cortical bone (CBA) was rehydrated in a bowel of sterile saline until implantation.

2.2. Preparation of animal for operation

Food and water was withheld for a period of twelve hours prior to the surgery. The pelvic limbs of all dogs were radiographed to document normal tibial anatomy. A prophylactic antibiotic course of Velosef (Squibb, Egypt) (500 mg) and Gentamycin (Alexandria Pharmaceutical Company, Alexandria, Egypt) (80 mg) was administered intravenously immediately preoperatively and continued twice a day for three days after surgery.

2.3. Anesthesia and control

All dogs were premedicated with I.V. injection of a mixture of atropine sulfate (Misr, Med. Company, Egypt) (0.05 mg/kg) and diazepam (Pharco Pharmaceuticals, Alexandria, Egypt) (1 mg/kg). Anaesthesia was induced immediately through I. V. injection of a mixture of Ketamine (Ketalar®: 5% Sol., Park-Davis and Co., U.S.A.) (10 mg/kg) and Xylazine (Rumpon®: 2% Sol., Bayer Leverkusen, Germany) (1 mg/kg). The anaesthetic depth was maintained with 2.5 % thiopental sodium (Biochemie GmbH, Vienna- Austria) administered intravenously (Schmidt-Oechtering and Alef, 1995)¹². The recipient dogs were restrained in lateral recumbancy.

2.4. Preoperative technique

The surgical site including the lower region of the hind limb (tibia) was prepared for aseptic surgery. Skin preparation consisted of clipping and shaving of hair, followed by at least three surgical scrubs with cotton and povidon iodine surgical scrubs for 10 minutes. This was followed by alcohol rinse and application of povidon iodine surgical spray that was allowed to dry for 2 to 3 minutes. Routine orthopedic operative draping and gowning procedures using towels stockinette and double surgical gloving were used during the operation.

2.5. Surgical procedure

A 7-cm incision was made in the medial surface of the tibia, extending through the periosteum, which was then reflected to expose the bone (MacNeill et al., 1999)¹¹. Four 6mm diameter defects were created using a sterile cylindrical drill bit under continuous sterile saline irrigation. Each defect extended through the cortex and into the cancellous bone. Packing the defect with gauze controlled hemorrhage from the medullary cavity. One defect was assigned by random selection to serve as the negative control (or simply Control), i.e., it was not filled. Two defects were assigned one of the two alloplastic graft materials, RBG or BGC, and the final defect was filled with allogenic cortical bone graft (CBA) (Fig. 1). The implantation site was flushed with sterile saline solution. The surgical wound was closed using polyglactin 910 (Vicryl®: Ethicon Ltd., U.K.) for close approximation of the adjacent muscles to the implanted bone. The subcutaneous tissue was sutured with Vicryl No. 2/0 and the skin incision was closed as usual.

2.6. Post-operative care:

All dogs were confined to individual cages for the duration of the study. The dogs were given milk and bread for the first 3 days post-operatively and then returned to normal diet within the first week. The skin sutures were removed 10 days post-operatively.

Conventional radiographs of two views (craniocaudal and mediolateral) were taken with a standard 30 x 40 cm film (MXB film, Eastman Kodak co., Rochester, New York, U.S.A.) at a 70 cm FFD, 48-52 kVp and 15 mAs in both craniocaudal and mediolateral positions (Toshiba, Model type: DXB-0324C5=A, Control panel model: KXO-15E Toshiba Corp., U.S.A.). All films were processed automatically under the same conditions using Kodak automatic processor (Model: M35X-Omat, Kodak, France). First radiographs were taken immediately post-operative, then follow

up examinations were performed a week later and at monthly intervals. For standardization a fixed distance was measured, starting at the farthest end of the animal's leg, and a point was marked. This point was placed at the center of the film each time. A step wedge was also used. Radiographs were evaluated for radiographic density of the alloimplants and control and for their degree of incorporation to the host bone. The conventional radiographs were scanned using a film digitizer (Acer Scan Prisa Model 620UT+, Acer Peripherals, Taiwan) into an IBM compatible computer (800 MHz PIII processor, 256 M Bytes of RAM, USB scanner interface) for further processing and analysis.

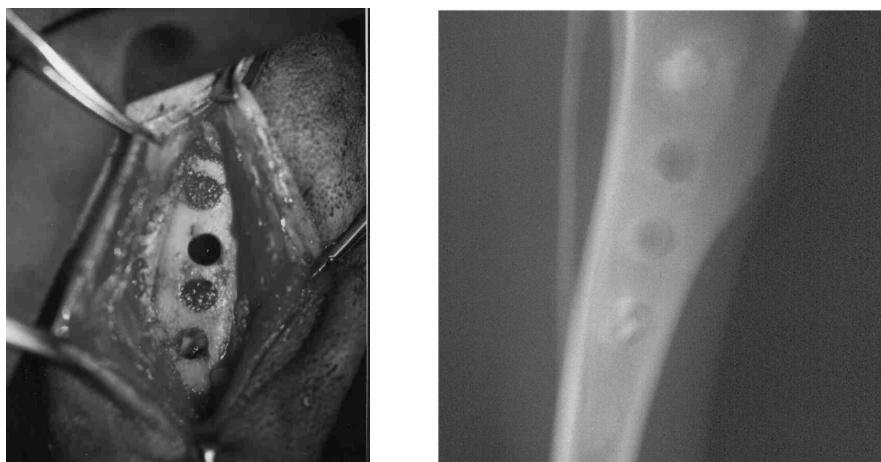


Figure 1. The surgical defects filled with the experimental materials (left) and their radiographic appearance (right).

3. IMAGE ANALYSIS

Since the acquired follow-up images during this study were distant apart in time, the imaging conditions cannot be assumed the same for all images. In particular, known variations in incident x-ray intensity as well as film processing must be accounted for in order to maintain consistency among all images. The strategy used here was to use a calibration step-wedge phantom as a reference to detect and correct fluctuations in digitized film intensity. The step-wedge phantom consists of three steps representing 2 mm, 4 mm and 6 mm of Aluminum. The phantom was placed near the imaged site in each of the acquired images. Fig. 2 shows a sketch drawing of the step-wedge phantom along with its radiographic appearance. After the film is digitized, the part of the image that contains the step-wedge is segmented and the average gray level in each step is obtained as the statistical mean of the histogram of values within this step. This is performed by asking the radiographer to select a box that lies entirely within the step-wedge part of the image. Then, the step levels are computed from the three distinct peaks that appear in the histogram of the pixels within this box as shown in Fig. 4. Once the three values representing the intensities of the steps of the phantom are computed, it is possible to correct the intensity of the whole image as follows.

Let the attenuation-free incident x-ray intensity be represented as I_0 and call those of the attenuated intensities after the three steps of the step-wedge as I_2 , I_4 and I_6 respectively. If we assume the effective attenuation per mm of Aluminum at the x-ray wavelength used as α , then the following equation applies for all images,

$$I_x = I_0 \cdot e^{-\alpha x} \quad (1)$$

Here, the values of I_0 and α are unknown, and x takes the values of 2, 4, and 6 mm. Since the value of α is not expected to vary in between images, we need to only compensate for the effect of I_0 . This can be as simple as eliminating α between any two of the three available equations and solving for I_0 . However, given the unavoidable presence of noise in our measurements, we need to devise a least-squares technique that allows the estimation of the unknowns in an optimal manner. This can be done by converting the equations obtained from (1) into a linear system by taking the natural logarithm of the equations to obtain a linear system of the form,

$$\begin{bmatrix} 1 & -2 \\ 1 & -4 \\ 1 & -6 \end{bmatrix} \cdot \begin{bmatrix} \log(I_o) \\ \alpha \end{bmatrix} = \begin{bmatrix} \log(I_2) \\ \log(I_4) \\ \log(I_6) \end{bmatrix}. \quad (2)$$

The linear system in (2) can be optimally solved to yield the following formulas for the unknowns,

$$I_o = \exp\left\{\frac{4}{3}\log(I_2) + \log(I_4) - \frac{2}{3}\log(I_6)\right\}, \quad (3)$$

and

$$\alpha = \frac{1}{4}\log(I_2) - \frac{1}{4}\log(I_6). \quad (4)$$

Therefore, for each image the values of I_o and α are computed using (3) and (4) and subsequently used to calibrate the intensity values of the whole image. This is accomplished by converting the intensity values into their equivalent Aluminum thickness using Eq. (1) such that,

$$x = \log\left(\frac{I_o}{I_x}\right) / \alpha. \quad (5)$$

Two problems associated with this idealistic methodology were encountered in our work. The first problem is how to determine the intensity values from the digitized radiographs given the nonlinearities in the relationship between incident x-ray energy and the density of the radiograph. On the other hand, the second problem is related to the variations in the processing methodology itself, which add baseline value to the whole radiograph as well as cause scaling of the range of gray levels that is difficult to predict in practice. An illustration of the obtained calibration values from a number of radiographs for the same dog is shown in Fig. 3. Notice the baseline differences between different images (manifested as the 0 mm value) and the variable compression of the range of values within the step-wedge phantom. Therefore, we resorted to a piecewise linear approximation of the relationship between equivalent Aluminum thickness and digitized film density. In particular, a given density is converted to an equivalent Aluminum thickness using linear interpolation between step-wedge values. The values outside the range of values of the step-wedge were computed based on extrapolation results based on polynomial modeling of the available density values. Even though this strategy is only approximate, its results were shown to be accurate based on measurements obtained from images obtained from the same dog at the same stage under different imaging and/or film development conditions.

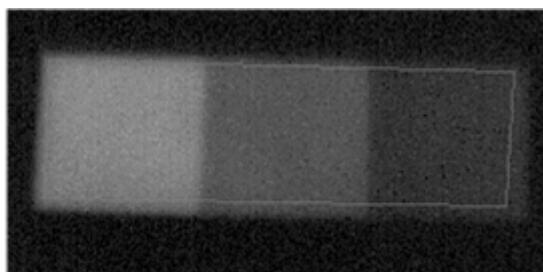
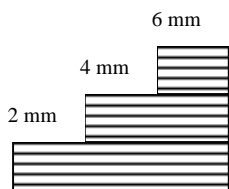


Figure 2. A sketch drawing of the step-wedge phantom used for image calibration (left) and its radiographic appearance (right).

Once the images are calibrated, the user-selected regions of interest are analyzed both qualitatively using subtraction radiography and quantitatively by computing a set of first and second order parameters from the pixels within the region of interest. The set of parameters used include the mean density, standard deviation, density percentiles, skewness, kurtosis, entropy, contrast, angular second moment, and correlation coefficient. The description of such parameters can be found in ¹³⁻¹⁴. The calibration/analysis programs were developed under IDL for windows v.5.2 (Research Systems, Inc.). Snapshots from the user interface of the developed programs are shown in Figs. 4 and 5. The developed software allows the user to open two images and globally align them for his/her convenience. Then, the calibration is performed and the user is allowed to select two regions of interest, one in each image, for further analysis. The program allows the user to obtain the subtraction radiograph of the selected regions and provides a host of tools to fine tune the subtraction

result through the elimination of relative affine motion between the two regions. The parameter set is calculated for each region separately and then used for further statistical analysis of the results.

4. RESULTS AND DISCUSSION

The progress in healing is illustrated in Fig. 6 where the uncalibrated radiographs at 6 different stages of this process are shown. The four circular areas from bottom to top represent RBG-, Control, BGC- and CBA-filled defects respectively. As can be observed, it is fairly difficult to assess the progress in the healing process just by looking at the radiograph given their different imaging and film development characteristics. The objective of this work is to characterize this progress in a quantitative manner. This is done by allowing the user to define the location of different spots for further analysis. Samples results obtained using the proposed system are shown in Figs. 7-9. As can be seen, the calibrated intensity of the operative lesions were calculated in the standard units of Aluminum thickness and plotted along the time line of the study. As can be seen, the results show the progress of the materials towards becoming a part of the bone structure over time in a far clearer manner than the visual inspection of the original radiographs. As indicated by the plots, different materials show different behavior in their approach to this baseline value. The identification of such differences between different materials is essential to the correct diagnosis of the progress in this healing process from radiographs. For example, it is possible in theory to assess the stage of a particular alloimplant given its radiograph by measuring the image parameters and comparing them to the stored database of evolution curves for each parameter over time. Hence, this can provide a valuable noninvasive diagnostic tool to assess the quality of healing and its extent.

5. CONCLUSIONS

A computer assisted radiological image characterization system was developed to evaluate alloimplant procedures from plain x-ray images. The developed system was designed using a carefully collected and analyzed data. The proposed methodology was evaluated and the results indicate its potential for assisting dental radiographers and surgeons in such important procedures. The main advantage of the proposed system is to help clinicians make more accurate evaluation of their surgical procedures as well as to guide them in selecting the most appropriate alloimplant material in an objective manner. Also, the developed system can be utilized routinely to assist dental radiologists reach an accurate diagnosis. Further investigation of its use in this application as well as in other clinical applications should be addressed.

REFERENCES

1. L.J. Peterson, E. Ellis III, J.R. Hupp, and M.R. Tucker, *Contemporary oral and maxillofacial surgery*, 3rd ed., Mosby, St. Louis, pp. 680-84, 1998.
2. P. F. van der Stelt, *Periapical bone lesions*, Thesis, Vrije Universiteit le Amsterdam, Naarden, Bock-er-Offsetrukkerij Los, 1979.
3. G. Revesz, H.L. Kundel and M.A. Graber, "The influence of structured noise on the detection of radiologic abnormalities," *Invest. Radiol.* **9**, pp. 479-486, 1974.
4. H.L. Kundel and G. Revesz, "Lesion conspicuity, structured noise, and film reader error," *Am. J. Roentgenol.* **126**, pp. 1233-1238, 1976.
5. B.G. Ziedses des Plantes, *Subtraction*, Stuttgart, Georg Theme Verlag, 1961.
6. C.K. Chow, S.K. Hilal and K.E. Niebuhr, "X-ray image subtraction by digital means," *IBM J. Res. Dev.* **17**, pp. 206-218, 1973.
7. C. Hardstedt and U. Welander, "Photographic subtraction. I. Theory of the subtraction image," *Acta Radiol. [Diagn.]* **16**, pp. 559-564, 1975.
8. C. Hardstedt, B. Rundellius, and U. Welander, "Photographic subtraction: Technical aspects and method," *Acta Radiol. [Diagn.]* **17**, pp. 101-106, 1976.
9. T.M. Lehmann, K. Gröndahl, H.-G. Gröndahl, W. Schmitt and K. Spitzer, "Observer-independent registration of perspective projection prior to subtraction of in vivo radiographs," *Dentomaxillofacial Radiology* **27**, pp. 140-150, 1998.
10. T. Lehmann, W. Oberschelp, E. Pelican and R. Repges, *Bildverarbeitung für die Medizin: Grundlagen, Modelle Methoden, Anwendungen*, Spriger-Verlag, Berlin, 1997.

11. S.R. MacNeill, C.M. Cobb, J.W. Rapley, A.G. Glaros, and P. Spencer, "In vivo comparison of synthetic osseous graft materials. A preliminary study," *Journal of Clinical Periodontology* **26**, pp. 239-245, 1999.
12. G. Schmidt-Oechtering, and M. Alef, "Neue aspekte der veterinaranasthesie und intensivtherapie," Blackwell wissenschafts-Verlag, Berlin, 1995.
13. Y.M. Kadah, A.A. Farag, J.M. Zurada, A.M. Badawi, and A.M. Youssef, "Classification algorithms for quantitative tissue characterization of diffuse liver disease from ultrasound images," *IEEE Trans. Medical Imaging* **15**, no. 4, pp. 466-478, 1996.
14. T.E. Southard and K.A. Southard, "Detection of simulated osteoporosis in maxillae using radiographic texture analysis," *IEEE Trans. Biomed. Eng.* **43**, no. 2, pp. 123-132, 1996.

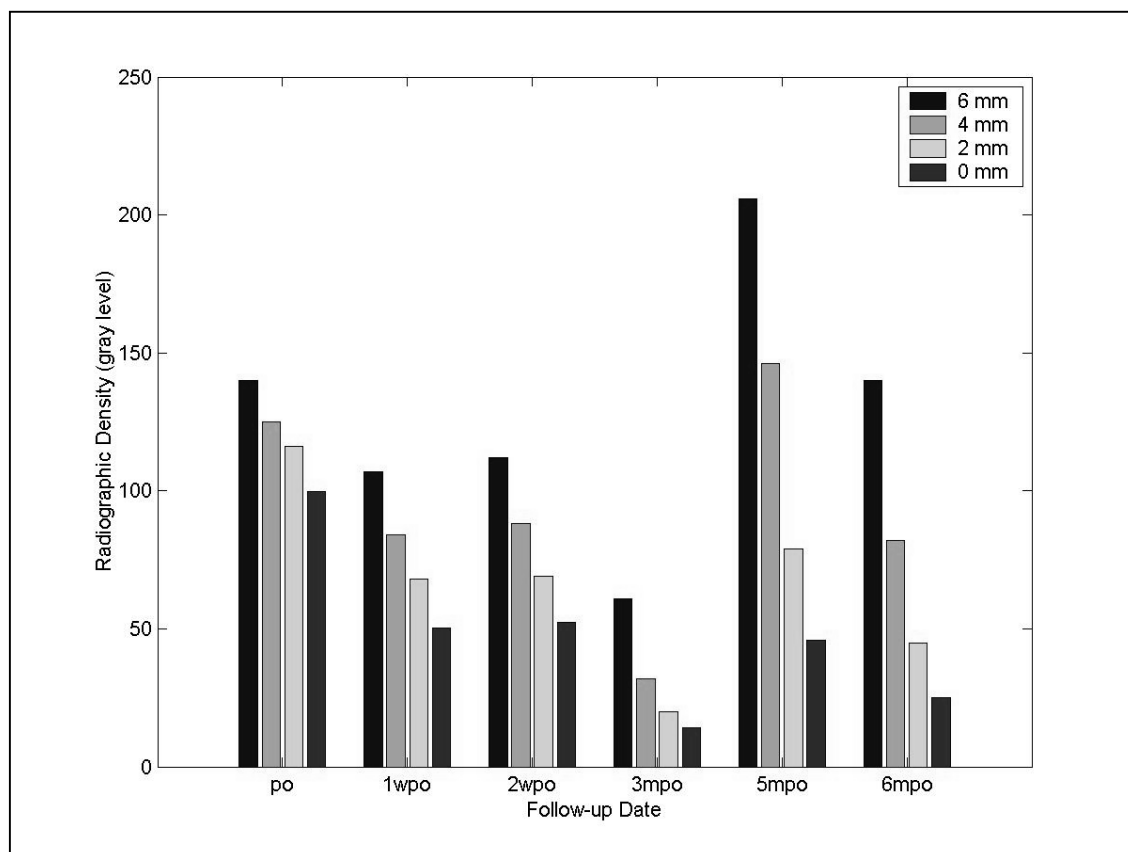


Figure 3. Measured calibration values from the step-wedge phantom (Aluminum thicknesses 2 to 6 mm) and the background of the x-ray image (assumed as the 0 mm Aluminum value). Notice the wide variations between different images from the same animal under different imaging and/or film development conditions.

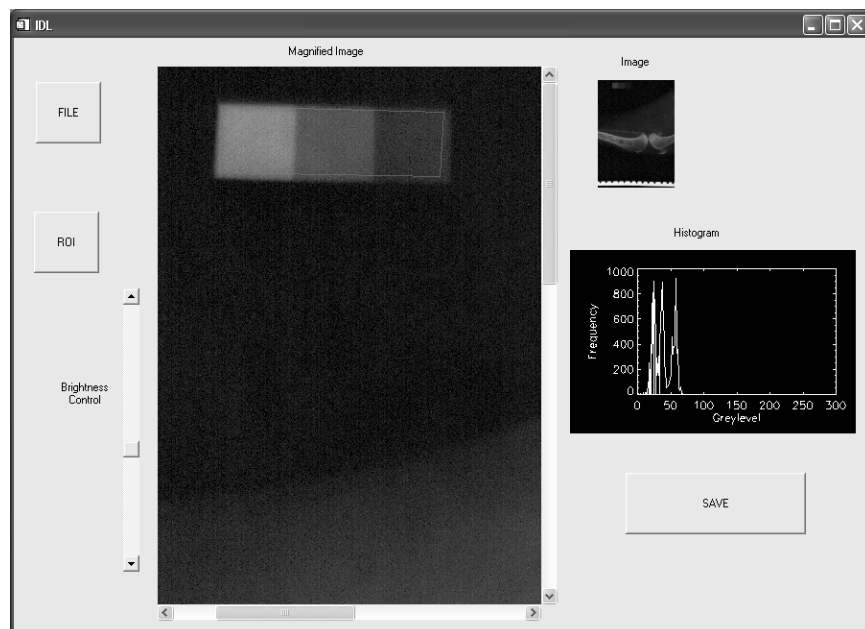


Figure 4. A snapshot for the user interface of the calibration program. The user opens an image and zooms into the area where the step-wedge is located in the image to select a region of interest within its boundaries for further analysis.

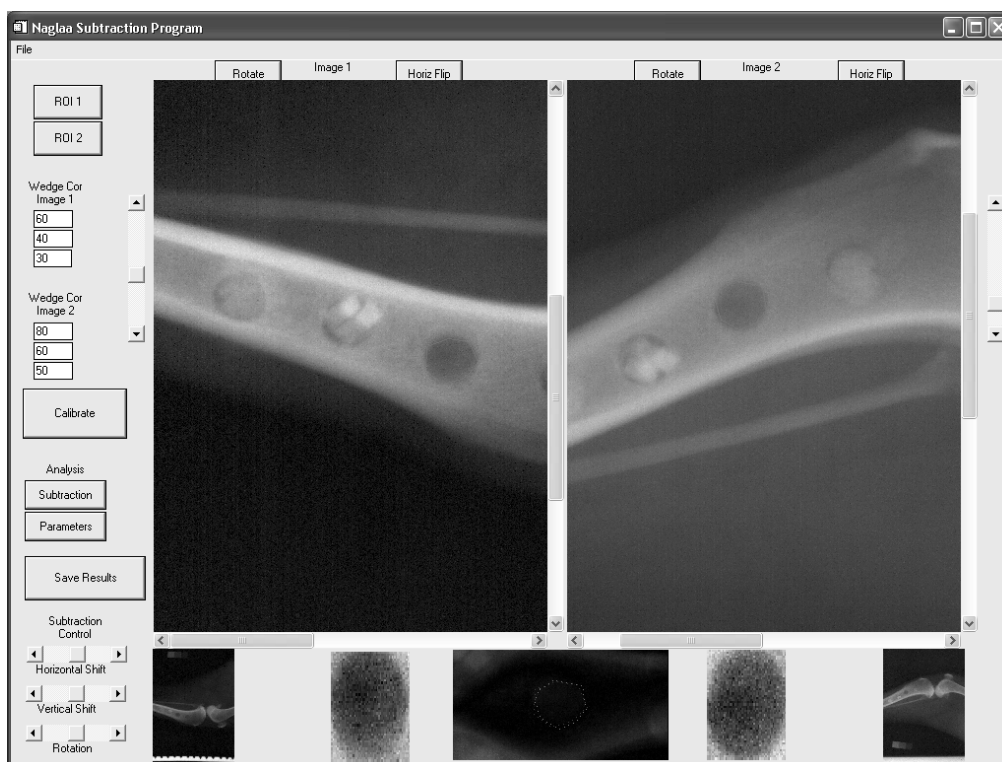


Figure 5. A snapshot of the analysis program where the user opens two images and manipulates them to produce a calibrated subtraction image and a set of parameters from each region of interest for further analysis.

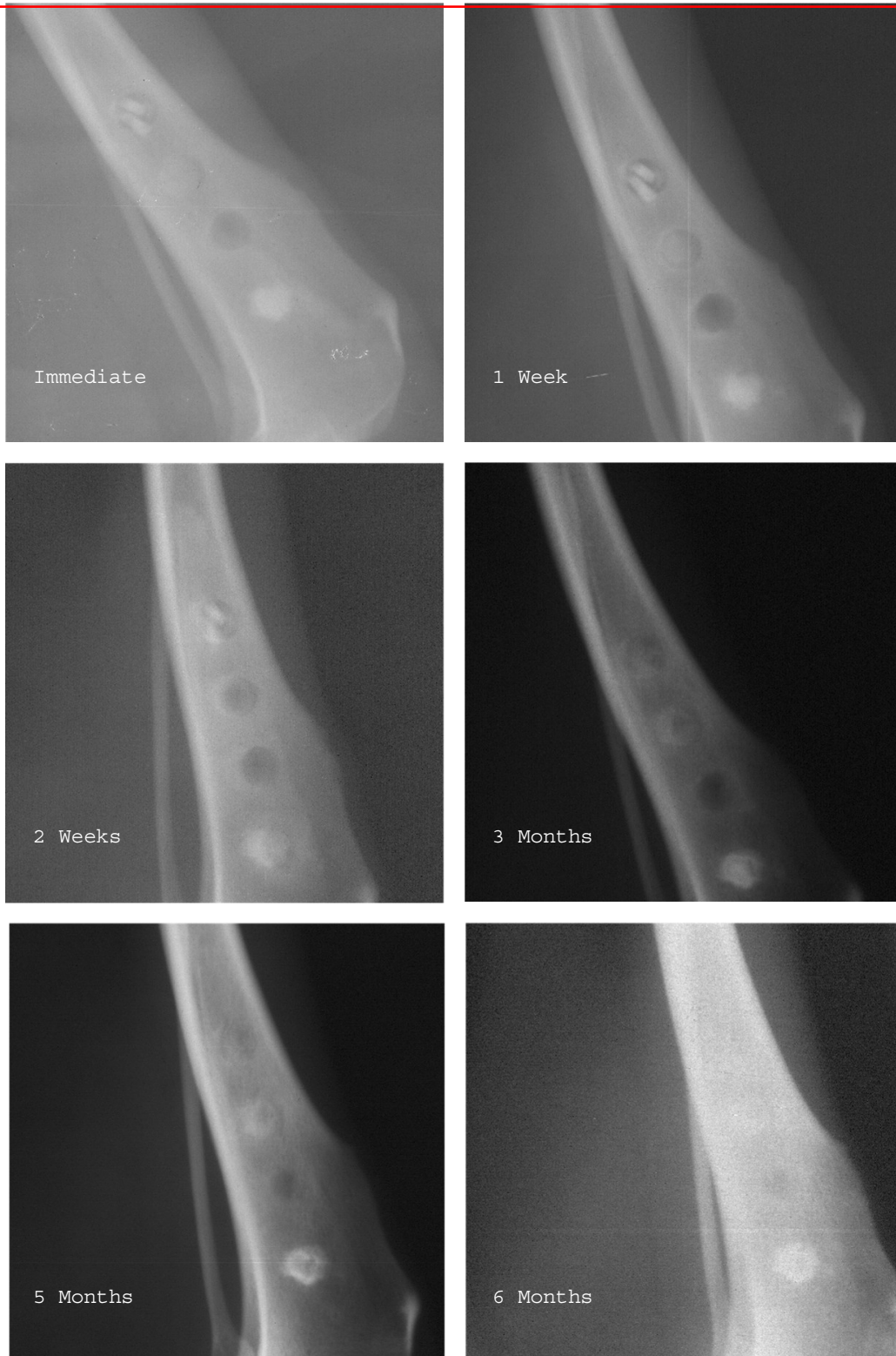


Figure 6. Illustration of the different stages in the healing process through radiographs of the same animal at different times. The four circular areas from bottom to top represent RBG-, Control, BGC- and CBA-filled defects respectively.

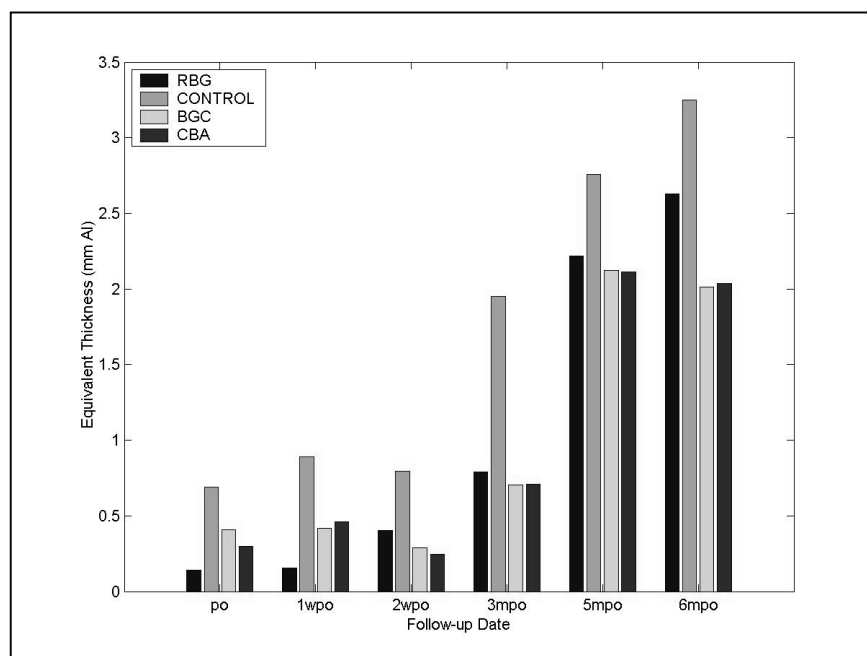


Figure 7. Results of mean region value expressed in absolute units of Aluminum thickness.

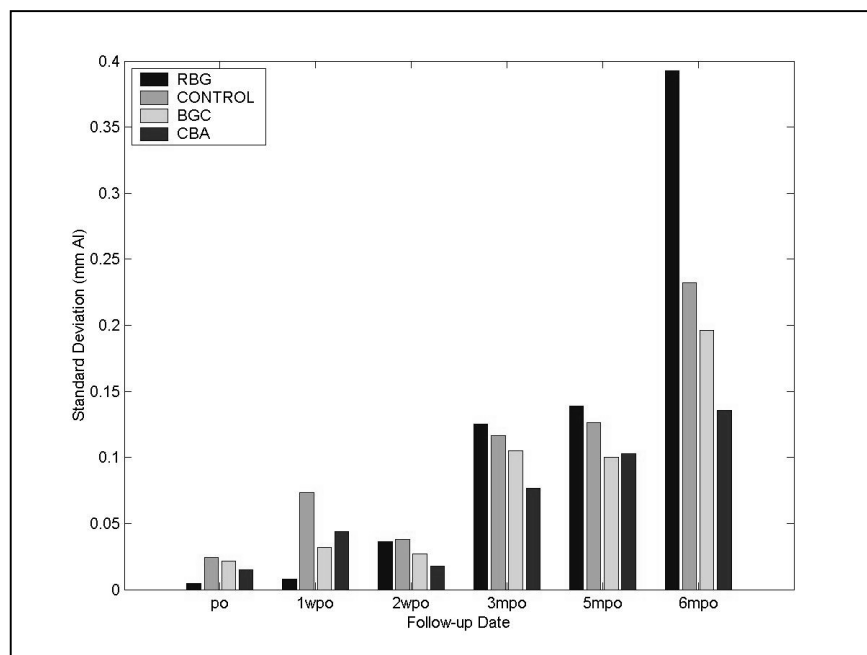


Figure 8. Results of standard deviation of region value expressed in absolute units of Aluminum thickness.

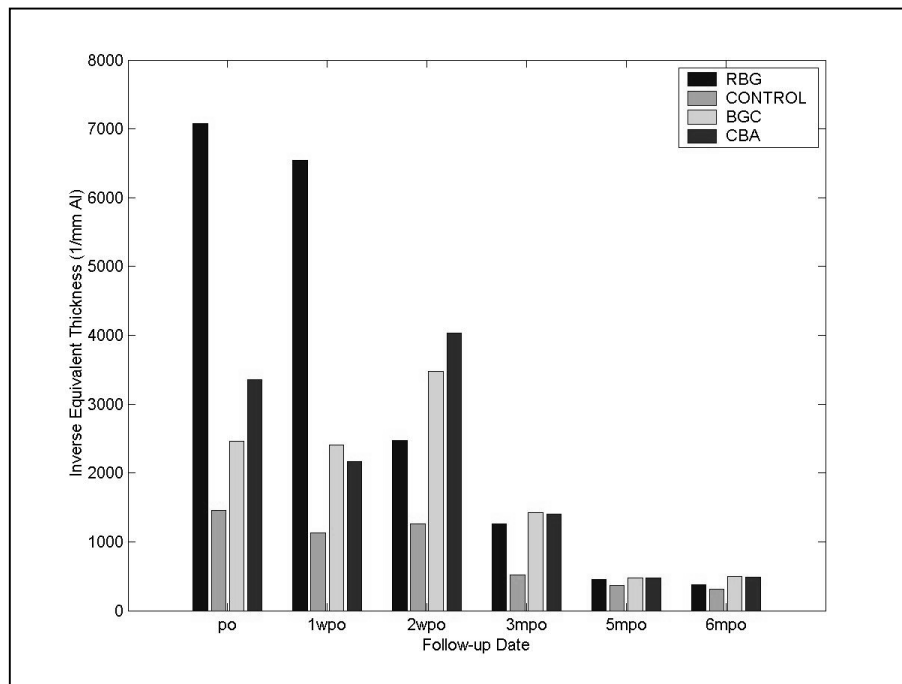


Figure 9. Results of mean region value expressed in invsrse of absolute units of Aluminum thickness.